This is an open access article published under a Creative Commons Non-Commercial No Derivative Works (CC-BY-NC-ND) Attribution License, which permits copying and redistribution of the article, and creation of adaptations, all for non-commercial purposes.

THE JOURNAL OF PHYSICAL CHEMISTRY A

Article

pubs.acs.org/JPCA

Parity-Dependent Rotational Energy Transfer in CN($A^2\Pi$, ν = 4, j $F_1\varepsilon$) + N_2, O_2, and CO_2 Collisions

Stephen J. McGurk, Joshua B. Halpern,‡ Kenneth G. McKendrick, and Matthew L. Costen*

Institute of Chemical Sciences, Heriot-Watt University, Edinburgh EH14 4AS, United Kingdom

ABSTRACT: We report state-resolved total removal cross sections and state-to-state rotational energy transfer (RET) cross sections for collisions of CN($A^2\Pi$, ν = 4, j $F_1\varepsilon$) with N_2, O_2, and CO_2. CN($X^2\Sigma^+$) was produced by 266 nm photolysis of ICN in a thermal bath (296 K) of the collider gas. A circularly polarized pulse from a dye laser prepared CN($A^2\Pi$, ν = 4) in a range of F_1e rotational states, j = 2.5, 3.5, 6.5, 11.5, 13.5, and 18.5. These prepared states were monitored using the circularly polarized output of an external cavity diode laser by frequency-modulated (FM) spectroscopy on the CN(A−X)(4,2) band. The FM Doppler profiles were analyzed as a function of pump−probe delay to determine the time dependence of the population of the initially prepared states. Kinetic analysis of the resulting time dependences was used to determine total removal cross sections from the initially prepared levels. In addition, a range of j' F_1e and j' F_2f product states resulting from rotational energy transfer out of the j = 6.5 F_1e initial state were probed, from which state-to-state RET cross sections were measured. The total removal cross sections lie in the order CO_2 > N_2 > O_2, with evidence for substantial cross sections for electronic and/or reactive quenching of CN(A, ν = 4) to unobserved products with CO_2 and O_2. This is supported by the magnitude of the state-to-state RET cross sections, where a deficit of transferred population is apparent for CO_2 and O_2. A strong propensity for conservation of rotational parity in RET is observed for all three colliders. Spin−orbit-changing cross sections are approximately half of those of the respective conserving cross sections. These results are in marked disagreement with previous experimental observations with N_2 as a collider but are in good agreement with quantum scattering calculations from the same study (Khachatrian et al. *J. Phys. Chem. A* **2009**, *113*, 3922). Our results with CO_2 as a collider are similarly in strong disagreement with a related experimental study (Khachatrian et al. *J. Phys. Chem. A* **2009**, *113*, 13390). We therefore propose that the previous experiments substantially underestimated the spin−orbit-changing cross sections for collisions with both N_2 and CO_2, suggesting that even approximate quantum scattering calculations may be more successful for such molecule−molecule systems than was previously concluded.

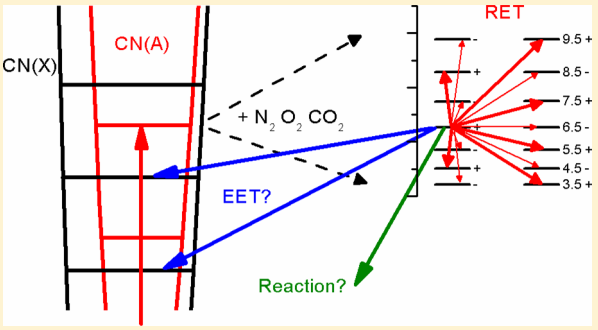

1. INTRODUCTION

Rotational energy transfer (RET) is a fundamental collisional process of importance in many gas-phase chemical environments, such as plasmas, combustion, and the atmosphere. Rotational state-to-state transfer cross sections or rate constants are crucial quantities for predictive modeling in such environments and as such have been the subject of numerous experimental and theoretical studies.[1,2] Radical species, particularly those possessing nonzero electronic orbital angular momentum, have been the subject of particular interest, notably NO($X^2\Pi$),[3−7] OH($X^2\Pi$),[8,9] and the subject of this work, CN($A^2\Pi$).[10−19] These radicals are not only among the most important chemical species in many of the environments of interest but also present challenges to experiment and theory arising from their electronic structure. The nonzero electronic orbital angular momentum of these $^2\Pi$ states results in both spin−orbit and Λ-doublet fine structure splitting of the rotational levels. The spin−orbit levels have body-frame projections of the angular momentum Ω = 1/2 or 3/2, labeled F_1 and F_2, with F_1 assigned to the lower in energy of the levels, which for CN($A^2\Pi$) is Ω = 3/2. The total rotational parity, p, depends on the rotational angular momentum, j, and the symmetry index ε of the Λ-doublet, via $p = \varepsilon(-1)^{j-1/2}$.[20] The Λ-doublets with ε = +1 are given the spectroscopic label e, while those with ε = −1 are labeled as f.[21] The total parity therefore alternates as a function of j within a particular Λ-doublet manifold, and e/f Λ-doublet pairs with the same j have the opposite parity. RET rate constants may be strongly dependent on the conservation or changing of either the spin−orbit state or the rotational parity.

RET in collisions with rare-gas (Rg) atoms has been the subject of the majority of experimental studies both because of the ease of experiments involving these partners and because such collisions may be investigated at the highest levels of theory. Accurate ab initio potential energy surfaces (PESs) may be generated, upon which exact quantum scattering (QS) calculations may then be performed. The approach of a spherical collider toward a $^2\Pi$ molecule results in two separate adiabatic PESs, of A′ and A″ symmetry with respect to reflection in the triatomic plane. In QS calculations, it is more

Received: December 17, 2013
Revised: February 12, 2014
Published: February 19, 2014

 © 2014 American Chemical Society dx.doi.org/10.1021/jp4123503 | *J. Phys. Chem. A* 2014, 118, 2007−2017

convenient to use the average sum and difference of these surfaces, with the V_{sum} and V_{dif} PESs defined as[20]

$$V_{sum}(R, \theta) = \frac{1}{2}[V_{A''}(R, \theta) + V_{A'}(R, \theta)] \quad (1)$$

$$V_{dif}(R, \theta) = \frac{1}{2}[V_{A''}(R, \theta) - V_{A'}(R, \theta)] \quad (2)$$

where R is the separation between the atom and the molecule center-of-mass and θ is the angle between **R** and the diatomic internuclear axis **r**. Within the Hund's case-(a) coupling limit, scattering within a single spin−orbit manifold is controlled by the anisotropic part of the V_{sum} PES, while the V_{dif} PES determines scattering between different spin−orbit manifolds.[20] For systems intermediate between Hund's case-(a) and case-(b), both the V_{sum} and V_{dif} PESs mediate the scattering within and between the different fine structure manifolds.[22] The angular dependence of the V_{sum} and V_{dif} PESs may also be conveniently expanded in terms of rotation matrix elements, $d^{\lambda}_{mm'}(\theta)$, and the radial coefficients $V_{\lambda 0}(R)$ and $V_{\lambda 2}(R)$, respectively.[20,22,23]

$$V_{sum} = \sum_{\lambda=0}^{\lambda_{max}} V_{\lambda 0}(R) d^{\lambda}_{00}(\theta) \quad (3)$$

$$V_{dif} = \sum_{\lambda=2}^{\lambda_{max}} V_{\lambda 2}(R) d^{\lambda}_{20}(\theta) \quad (4)$$

Inspection of the matrix elements of the interaction potentials expanded in this form reveals that rotational parity-conserving collisions result from the even-λ terms of the expansion, whereas parity-changing collisions arise from the odd-λ terms, within a weak-coupling limit.[22−24]

The CN($A^2\Pi$) + Ar system has been one for which RET has been intensively studied by both experiment and QS theory.[12,17−19] We have recently collaborated with Dagdigian, Alexander, and co-workers in a combined experimental and theoretical study.[10,11] Using the same basic experimental approach as that used to obtain the results presented in this paper, CN($A^2\Pi$, ν = 4, j Fε) was prepared by optical pumping in a thermal (296 K) bath of Ar. The total removal rate constants for different initial states and the state-to-state rate constants for transfer to a range of CN($A^2\Pi$, ν = 4, j' $F'\varepsilon'$) product states were determined by optical probing. Rapid total removal rate constants, typically on the order of 4×10^{-10} cm^3 s^{-1}, were observed, very close to those reported by Yang et al. in an earlier study of the corresponding rotational state in the adjacent vibrational level CN(A, ν = 3) with Ar.[17] QS calculations on new ab initio PESs reproduced the trends in total removal rate constants well, albeit with a small systematic overprediction relative to experiment of ∼10−15%.[11] The state-to-state population transfer rate constants were determined starting from two initial states, j = 6.5 F_1e and j = 10.5 F_2f, in each case to a range of j' F_1e and j' F_2f product states.[10] Excellent agreement between experiment and theory was seen. The RET rate constants displayed the almost universal strongly decreasing trend in magnitude with increasing Δj, resulting from linear-to-angular momentum transfer restrictions.[25,26] However, strong parity-dependent oscillations were superimposed on this trend, with a marked preference for rotational parity conservation being observed. Overall, it is clear that current theory can provide essentially near-quantitative agreement with experiment for this benchmark $^2\Pi$ + Rg system.

In contrast to the extensive work on CN(A) + Rg, experimental measurements of energy transfer of CN(A) in collisions with molecular colliders are much rarer. Vibrational state-resolved rate constants for removal of CN(A), k_Q, have been reported for N_2, O_2, CO_2, ClCN, and C_2N_2. Both for molecules and Rg atoms, rate constants increase with the CN(A) vibrational quantum number and with the mass and length of the collision partner.[27−29] We distinguish in what follows between the total removal from the A state, total quenching, k_Q, and its components: electronic energy transfer (EET), resulting in CN(X); and reaction of CN(A) with the collider to form some unobserved products. Different colliders may display not only different total quenching rate constants but also different partitioning of the total into EET or reaction. We note that, in principle, vibrational relaxation within the A state could contribute to k_Q as defined, but in practice, it has been shown to be an insignificant process. Studies of state-to-state RET have been limited to collisions with H_2, N_2, CO_2, and CH_4.[13,14,30,31] An open question with these molecular colliders is what effect, if any, the presence of the EET or reactive channels has on the observed RET within the excited state.

Most relevant to the work presented here are the combined experimental and theoretical investigations of CN(A) + N_2 RET by Dagdigian, Alexander, and co-workers and the experimental study of CN(A) + CO_2/CH_4 by Khachatrian and Dagdigian.[13,14] In each case, they used optical−optical double resonance (OODR) to measure fully state-resolved j Fε to j' $F'\varepsilon'$ RET rate constants of low-j CN($A^2\Pi$, ν = 3). In addition, for CN(A)−N_2, they calculated ab initio PESs for three limiting orientations of the CN and N_2 and subsequently performed QS calculations on spherically averaged PESs constructed from these limiting cases. A marked disagreement between experiment and theory was reported for CN(A) + N_2 in both the relative propensities for scattering into different spin−orbit and Λ-doublet manifolds and the relative Δj propensities within specific fine structure manifolds. The theoretical results strongly resemble in general form those previously reported for both experiment and theory for CN(A) + Ar collisions.[10,18] In contrast, the experimental results showed a very strong preference for spin−orbit and Λ-doublet conservation. Dagdigian, Alexander, and co-workers discuss this remarkable disagreement between experiment and theory in terms of a failure of the theory, suggesting that this is a result of the simplifications imposed by the spherical averaging of the CN(A)−N_2 PESs and neglect of the rotation of the N_2. The separate experimental measurements of RET with CO_2 and CH_4 as colliders also showed a very strong preference for spin−orbit and Λ-doublet conservation.[14]

The current paper provides new measurements of rotationally inelastic collisions of CN($A^2\Pi$) with two of the molecular partners studied by Khachatrian et al., namely, N_2 and CO_2, together with the previously unstudied O_2. Together, these provide a range of total A state removal rate constants while having similar collision kinematics. We apply OODR using the frequency-modulated spectroscopy (FMS) techniques that we have previously applied to CN(A) + Ar collisions[10−12] to measure the total removal rate constants for CN($A^2\Pi$, ν = 4, j = 2.5, 3.5, 6.5, 11.5, 13.5, and 18.5 F_1e) with N_2, O_2, and CO_2, together with state-to-state transfer rate constants from j = 6.5 F_1e to j' F_1e and j' F_2f final levels. We compare these new results to both our previous measurements of total removal and state-to-state rate constants for CN(A) + Ar, as well as the experimental measurements and theory presented by Khacha-

dx.doi.org/10.1021/jp4123503 | J. Phys. Chem. A 2014, 118, 2007−2017

trian et al.[13,14] As we will show, our results provide new and accurate measurements for the total removal of CN(A) by molecular colliders, confirming that additional loss channels are present for O_2 and CO_2 that are absent for Ar and N_2. The state-to-state propensities suggest strongly that a reappraisal is needed of the apparent inability of ab initio calculations to reproduce the previous experimental results for molecular collision partners.

2. EXPERIMENTAL METHODOLOGY

The experimental apparatus has been described in detail previously.[10−12,15,16,32] The experiments were performed in a 2 m longitudinal vacuum chamber, within a region shielded by a μ-metal cylinder to isolate the sample from stray magnetic fields.[33] A 10 sccm mass flow controller (Aera) provided a slow flow of collider gas (N_2 or O_2 research grade >99.9995%, CO_2 research grade >99.999%, BOC Gases), which carried ICN (Acros Organics, 98%) into the vacuum chamber. The collider gases were supplied directly from their respective cylinders, using independent and unconnected gas lines to avoid any possibility of cross-contamination. The diffusion pump that evacuated the chamber was throttled by a gate valve to provide a pressure of ∼30 mTorr with a typical 1:5 mixture of ICN to collider. Additional collider gas was then added via a second mass flow controller (MKS Instruments, 100 sccm). For the population removal experiments, the total pressure was varied between 100 and 1000 mTorr. In the RET experiments, the total pressure was maintained at 400 ± 5 mTorr for N_2 and O_2 and 200 ± 5 mTorr for CO_2. Pressures were monitored using a 0−10 Torr capacitance manometer (MKS Instruments).

The ICN was photolyzed at 266 nm using a Nd:YAG laser (Continuum Surelite III-10) to produce CN($X^2\Sigma^+$, ν = 0). For experiments using N_2 and CO_2, a post-photolysis delay of 30 μs ensured thermalization of the substantial nascent translational and rotational energy and also ensured that the strong rotational alignment of CN(X) produced in this photolysis was destroyed.[32,34] Reaction of CN(X) with O_2, $k_{298} = 5 \times 10^{-11}$ cm^3 s^{-1}, is fast enough to lead to a substantial loss of CN(X) during a 30 μs delay at the higher collider pressures.[35] The photolysis pump delay was therefore varied with collider pressure to maintain a constant collision number (∼5 RET collisions) for experiments involving O_2, chosen to give the best compromise between translational and rotational thermalization while limiting the reactive loss of CN(X).

The strongly saturating output (∼65 mJ cm^{-2}) of a Nd:YAG pumped dye laser (Spectron SL803/SL4000) was copropagated along the photolysis beam and tuned to selected lines of the R_1 branch of the CN $A^2\Pi-X^2\Sigma^+$ (4,0) band at around 620 nm to prepare CN($A^2\Pi$, ν = 4, j = 2.5, 3.5, 6.5, 11.5, 13.5, and 18.5 F_1e). The transitions chosen were sufficiently isolated that no significant excitation of other CN(A, ν = 4) rotational states was observed. The pump beam polarization was switched between left- and right-handed circular by a photoelastic modulator (PEM-80, Hinds Inc.) immediately before the vacuum chamber. The timing of the photolysis and pump laser pulses relative to the PEM compression cycle was controlled by a digital delay generator (SRS DG535) under experimental software control.

Both the initially prepared CN($A^2\Pi$, ν = 4, j = 2.5, 3.5, 6.5, 11.5, 13.5, and 18.5 F_1e) levels and the product ($|\Delta j| \leq 5$) CN($A^2\Pi$, ν = 4, j' Fε) levels of RET from j = 6.5 F_1e were probed by frequency-modulated (FM) SE using an external cavity tunable diode laser (Sacher GmbH, TEC520) on selected R_1, P_2, and R_2 + $^PQ_{21}$ rotational transitions of the $A^2\Pi-X^2\Sigma^+$ (4,2) band between 827 and 835 nm. The FM probe beam counterpropagated the photolysis and pump beams in a double-pass configuration and was detected by a 1 GHz photoreceiver (New Focus, 1601FS-AC). The probe laser beam was step-scanned across the transition of interest in 100 MHz increments, and the transient in-phase (I) and quadrature (Q) signals were independently averaged (20−50 laser shots) using a digital storage oscilloscope (LeCroy LT342). A scanning Fabry−Perot interferometer (CVI Technical Optics, free spectral range of 2 GHz) was used to monitor the modulated diode beam, and the recorded output was subsequently used to linearize the frequency scale of the spectra.

The FM probe beam was circularly polarized, and therefore, the switching of the pump laser polarization between right- and left-handed circular gave two experimental geometries, termed corotating (co) and counter-rotating (con). The photolysis of ICN at 266 nm produces a small fraction of the CN $X^2\Sigma^+$ in ν = 2, resulting in a background absorption signal.[36] Additional background transient signals were therefore acquired at each wavelength step in the absence of the pump pulse. The number of frequency steps required to scan the transition of interest was 50−60, which, with the four-fold delay settings described, typically took approximately 20 min. For population removal experiments, scans were acquired at varied collider pressures without alteration of any other experimental conditions, with the exception of minor reoptimization of the pump laser frequency, where slow thermal drifts away from the pump transition frequency were observed on a time scale of 1−2 h. The collider pressures were varied in a pseudorandom fashion. In the population transfer experiments, multiple product levels were probed in a single experimental session. To minimize systematic errors arising from slow drifts in the pump laser wavelength, spectra were acquired alternately for the prepared and the product states for the population transfer experiments, with the pump laser wavelength reoptimized whenever necessary. Spectra from multiple product levels were then acquired in uninterrupted experimental sessions lasting typically 4 h, during which either all of the spin−orbit-conserving or spin−orbit-changing transitions were independently probed. In addition, some sessions were used to acquire a mix of spin−orbit-conserving and -changing transitions to allow direct comparison. Product levels were acquired in pseudorandom sequence, and the experiments were repeated until each product level had been probed a minimum of four times.

3. RESULTS

The use of polarized lasers to prepare and probe rotational states necessarily results in the preparation and probing of rotational angular momentum polarization. Although the focus of this paper is population transfer, we need to analyze the experimental data including polarization effects in order to isolate the desired population information. Polarization effects will be reported separately. We have followed the approach that we have described in previous publications on the CN(A) + Ar system.[10,11]

The one-photon linear FM probe method is only sensitive to rotational polarization tensor moments of rank K = 0, 1, and 2,[37] and in an isotropic collision environment, moments of different rank cannot mix.[38] Optical excitation imposes cylindrical symmetry upon the prepared distribution, and hence, the observed signal depends on population, $A_0^{(0)}$, orientation, $A_0^{(1)}$, and alignment, $A_0^{(2)}$, moments. The two

dx.doi.org/10.1021/jp4123503 | J. Phys. Chem. A 2014, 118, 2007−2017

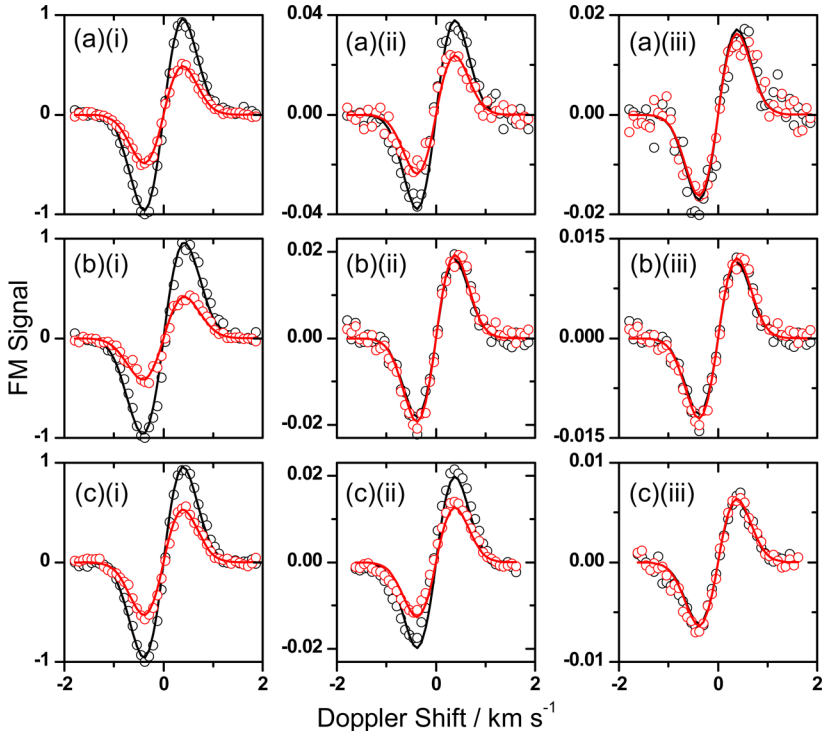

Figure 1. Representative data (circles) and fits (lines) for the SE FM line shapes for corotating (black) and counter-rotating (red) geometries. (i) j = 6.5 F_1e initial state; (ii) $\Delta j = -2$ spin−orbit- and Λ-doublet-conserving; (iii) $\Delta j = -2$ spin−orbit- and Λ-doublet-changing product states for (a) N_2, (b) O_2, and (c) CO_2 colliders. For the purposes of presentation, the first 100 ns of postpump signals have been averaged.

pump−probe geometries used in this work (co and con) have integral intensities, I_{co} and I_{con}, given in eq 5, where the (+) sign refers to I_{co} and the (−) sign to I_{con}.

$$I_{(co)(con)} = \frac{ES}{3(2j+1)}A_0^{(0)}\left[1(\pm)\frac{3}{2}h^{(1)}(j)A_0^{(1)} - \frac{1}{2}h^{(2)}(j)A_0^{(2)}\right] \quad (5)$$

The experimental sensitivity to parameters such as optical path length, absolute number density, and detector response is contained in the parameter E; S is the rotational line strength factor, and $h^{(K)}(j)$ is the rotational branch sensitivity to the moment of rank K.[39,40] As we have previously shown, with the strong saturation involved in our pump step and the use of circular pump polarization, the alignment moment $A_0^{(2)}$ makes a negligible contribution to the measurements in these two geometries, and we have consequently set this term to zero in the subsequent analysis.[10]

The experimental data were analyzed as FM Doppler line shapes in custom-written LabVIEW routines. The acquired FM background 2-d arrays were first subtracted from the corresponding signal arrays for each experimental geometry. The background-subtracted I and Q arrays were then rotated to yield pure stimulated emission (SE) and dispersion (D) arrays.[41] FM Doppler line shapes for sequential 10 ns averages of the SE and D signals for each geometry were constructed, with the wavelength scale linearized using the acquired monitor etalon traces.

Gaussian Doppler profiles for the two geometries were simulated for assumed $A_0^{(0)}$ and $A_0^{(1)}$ moments with intensities given by eq 5. The simulated profiles were then transformed into FM SE and D line shapes and simultaneously least-squares fitted using the Levenberg−Marquardt (LM) method to the experimental FM line shapes, optimizing the $A_0^{(0)}$and $A_0^{(1)}$ moments and, where appropriate, the translational temperature (for transferred states, the translational temperature was fixed at 296 K). This Doppler profile analysis resulted in the time dependence of the population and orientation, providing kinetic traces for subsequent fitting. As previously noted, the orientation elastic depolarization and orientation state-to-state transfer efficiencies will be the subject of a future publication and are not reported here.

Representative data and fits for the SE FM line shapes are shown for the j = 6.5 F_1e prepared state and example $\Delta j = -2$ spin−orbit- and Λ-doublet-conserving and spin−orbit- and Λ-doublet-changing product states in Figure 1. For the purposes of presentation, the first 100 ns of postpump signal has been averaged.

We determined the total population removal rate out of the initial level, $\Gamma_{j,tot}^{(0)}$, by fitting the data to a simple three-level kinetic model, previously used to fit CN(A) + Ar population removal kinetics.[11] The three levels are the initial level, j; a product level from which return to j is possible, j', representing levels similar in energy and angular momentum to j; and product level j_x, representing levels from which return to j is not possible. These j_x levels may be within the same vibrational state as j and j' and be distant in rotational energy and/or angular momentum, but this channel also includes vibrational relaxation within CN(A) (known to be a minor contributor), electronic quenching and fluorescence to the $X^2\Sigma^+$ state, reaction to unobserved products, and the loss of the initial population through "fly out" from the probed volume. The total removal rate is given by the sum of the individual rates for transfer from j to j', $\Gamma_{j\to j'}^{(0)}$ and to j_x, $\Gamma_{j\to x}^{(0)}$

$$\Gamma_{j,tot}^{(0)} = \Gamma_{j\to j'}^{(0)} + \Gamma_{j\to x}^{(0)} \quad (6)$$

dx.doi.org/10.1021/jp4123503 | J. Phys. Chem. A 2014, 118, 2007−2017

The population removal measurements were repeated for typically 10 different collider pressures between 100 and 1000 mTorr. For the RET experiments, as discussed in the Experimental Methodology section, alternating measurements of the initial state and selected product states were performed under conditions in which all other experimental parameters were held constant. This ensured that absolute signal sizes acquired during each experimental session were directly comparable. We restricted the fitting of the population transfer to short delays (≤250 ns) where single-collision conditions were assumed. We first fitted the population removal from the initial level to the three-level kinetic model to determine $\Gamma^{(0)}_{j,\mathrm{tot}}$. This result was then used in a fit of eq 7 to the product level kinetic trace to determine the state-to-state population transfer rate, $\Gamma^{(0)}_{j\rightarrow j'}$, where here j' can be identified as the single product state detected in the probe spectroscopic step.[10]

$$A_0^{(0)}(j';\, t) = A_0^{(0)}(j;\, t=0)\left[\frac{\Gamma^{(0)}_{j\rightarrow j'}}{\Gamma^{(0)}_{j,\mathrm{tot}}}\right](1 - \mathrm{e}^{-\Gamma^{(0)}_{j,\mathrm{tot}}t}) \tag{7}$$

The measurements of the initial level that bracketed the product level measurement were used to perform independent fits of each product level, and the results were averaged.

All fitting was performed using custom-written LabVIEW routines, using LM minimization with weighting by the statistical deviation of the data. Figure 2 shows representative kinetic traces and fits for the total removal of population from the initial level $j = 6.5\ F_1e$ at several pressures and the state-to-state population transfer for $\Delta j = -1$ and -2, spin−orbit- and Λ-doublet-conserving and -changing, respectively, for each collider. The multiple traces in each panel of Figure 2a−c(i) show, as expected, more rapid removal of population from the initial level with increasing collider pressure. The traces in Figure 2a(i) and b(i) are very similar, indicating similar total removal kinetics for N_2 and O_2, although close inspection reveals that the kinetic traces for O_2 tend to zero at long times, while a near-constant nonzero background is present for N_2. In contrast, total removal with CO_2 is clearly markedly faster than that with N_2 and O_2, and the traces also tend to zero at long times. The different long-time behavior of the traces for N_2 and O_2 suggest that while their total removal rate constants are similar, the breakdown of that rate between RET and other removal processes, for example, quenching, is different. For CO_2, the long-time behavior also suggests that non-RET processes are significant. In contrast to the prompt appearance of the directly prepared signals in Figure 2a−c(i), the kinetic traces in Figure 2a−c(ii,iii) display the more gradual rise times expected for the products of RET, confirming that the population observed for these levels arises solely from RET from the prepared $j = 6.5\ F_1e$ level.

Bimolecular rate constants, k_{pop}, for the total removal were determined from conventional second-order plots of the measured total removal rates, $\Gamma^{(0)}_{j,\mathrm{tot}}$, as function of collider number density, $[N]$, with linear fits to eq 8

$$\Gamma^{(0)}_{j,\mathrm{tot}} = k_{\mathrm{pop}}[N] + \Gamma^{(0)}_{j,\mathrm{tot,int}} \tag{8}$$

where the intercept is the zero-pressure total removal rate, $\Gamma^{(0)}_{j,\mathrm{tot,int}}$, resulting from collisions with the precursor ICN and noncollisional processes, such as fly out from the probed region and radiative loss. Examples of these plots for population removal out of $j = 6.5\ F_1e$ and $j = 11.5\ F_1e$ are shown in Figure 3

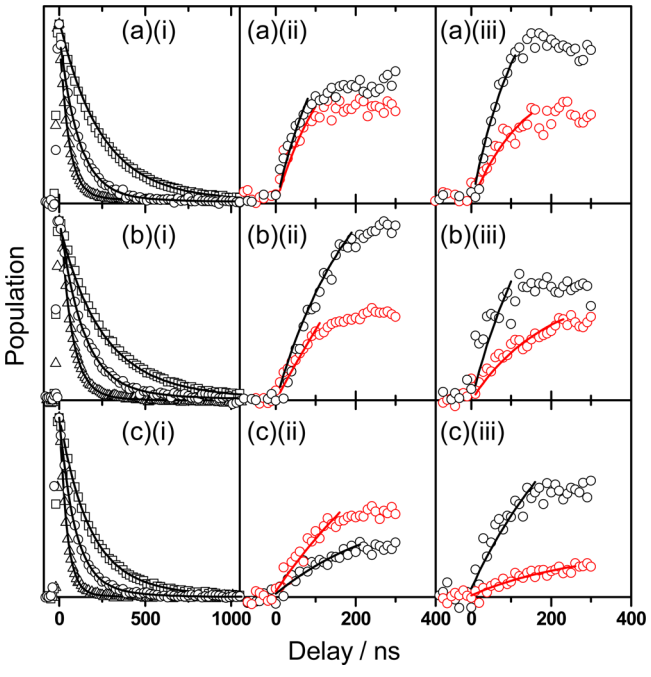

Figure 2. Kinetic traces and fits for the three colliders: (a) N_2, (b) O_2, and (c) CO_2. (i) Total population removal from $j = 6.5\ F_1e$ at ∼200 (squares), ∼400 (circles), and ∼1000 mTorr (triangles). Products of state-to-state population transfer (multiplied by a factor of 30) for (ii) $\Delta j = -1$ and (iii) $\Delta j = -2$. (Black) Spin−orbit- and Λ-doublet-conserving, (red) spin−orbit- and Λ-doublet-changing at 400 mTorr of pressure for N_2 and O_2 and 200 mTorr for CO_2. Experimental uncertainties have been omitted for clarity.

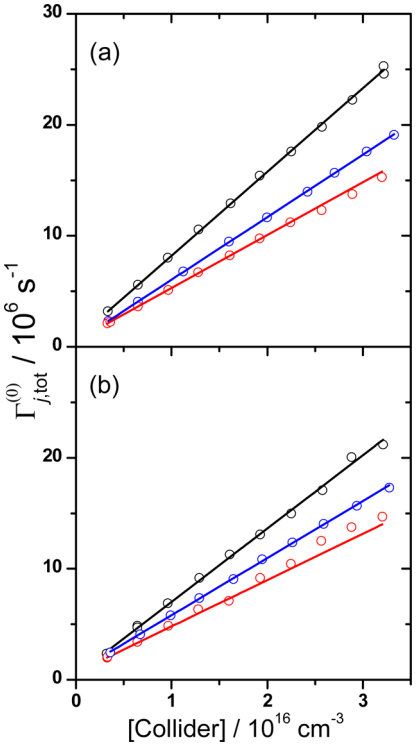

Figure 3. Total population removal rates, $\Gamma^{(0)}_{j,\mathrm{tot}}$, as a function of collider number density, with linear fits. (a) $j = 6.5\ F_1e$ and (b) $j = 11.5\ F_1e$ for N_2 (blue), O_2 (red), and CO_2 (black) colliders. Experimental uncertainties have been omitted for clarity.

dx.doi.org/10.1021/jp4123503 | J. Phys. Chem. A 2014, 118, 2007−2017

for each collider. Figure 3 clearly shows that the total removal rate constants are well-determined and lie in the order CO_2 > N_2 > O_2. The intercept rates, $\Gamma^{(0)}_{j,\mathrm{tot,int}}$, are typically ~5.0 × 10^5 s^{-1}, consistent with the radiative rate (2.6 × 10^5 s^{-1}) and a modest contribution from fly out.[27]

The population removal rate constant for each collider, k_{pop}, was turned into a thermally averaged cross section, σ_{pop}, according to eq 9

$$\sigma_{\mathrm{pop}} = \frac{k_{\mathrm{pop}}}{\langle v_{\mathrm{rel}} \rangle} \tag{9}$$

where $\langle v_{\mathrm{rel}} \rangle$ is the average relative velocity of the collision partners, to allow direct comparison of the population removal kinetics, independent of trivial differences in the total rate of collisions, as shown in Figure 4. The total removal cross

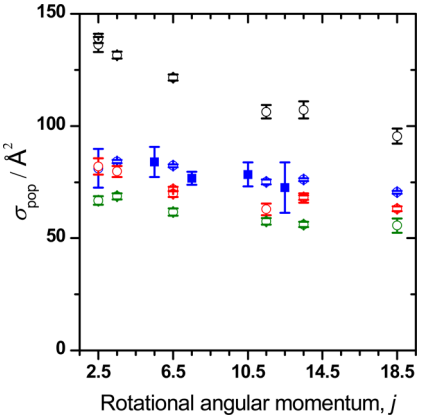

Figure 4. (Open circles) Total population removal thermally averaged cross sections, σ_{pop}, for different CN($A^2\Pi$, ν = 4, j, F_1e) levels for N_2 (blue), O_2 (red), and CO_2 (black circles) colliders. The cross sections are also compared to our previous measurements with Ar (olive circles) from ref 11. Errors are 2σ from the fits to eq 8. (Filled squares) σ_{pop} for different CN($A^2\Pi$, ν = 3, j F_1f) levels for the N_2 collider from ref 13.

sections, including the previous data for Ar,[11] are found to lie in the order Ar < O_2 < N_2 < CO_2 irrespective of j. For all of the colliders, there is a general decline in total removal cross section as a function of increasing j, with this trend being somewhat stronger for CO_2.

Becuse the kinetic traces for different colliders showed different long-time behavior, as shown in Figure 2, we have also performed bimolecular fits to the individual rates $\Gamma^{(0)}_{j\rightarrow j'}$ and $\Gamma^{(0)}_{j\rightarrow x}$ that make up $\Gamma^{(0)}_{j,\mathrm{tot}}$, as well as the return rate $\Gamma^{(0)}_{j'\rightarrow j}$, and have determined the resulting rate constants and thermally averaged cross sections. Figure 5 presents these bimolecular plots for the initial states j = 6.5 F_1e and j = 11.5 F_1e for all four colliders, where the Ar data are from our previous measurements.[11] Figure 5a(i,ii) and b(i,ii) shows that for both states, for Ar and N_2, the total removal rate, $\Gamma^{(0)}_{j,\mathrm{tot}}$, is dominated by the contribution from reversible transfer, $\Gamma^{(0)}_{j\rightarrow j'}$. In contrast, in Figure 5c(i,ii) and d(i,ii), a substantial contribution to $\Gamma^{(0)}_{j,\mathrm{tot}}$ is made by irreversible loss for O_2 and CO_2, $\Gamma^{(0)}_{j\rightarrow x}$.

Figure 6 shows the breakdown of σ_{pop} into the contributions from the best-fit removal cross sections, $\sigma^{(0)}_{j\rightarrow j'}$ and $\sigma^{(0)}_{j\rightarrow x}$, for each rotational level studied, for each collider, including results for Ar derived from the previously published data.[11] The return cross sections, $\sigma^{(0)}_{j'\rightarrow j}$, were determined to be small, typically between 1 and 5 Å^2, in essentially all cases and are not shown.

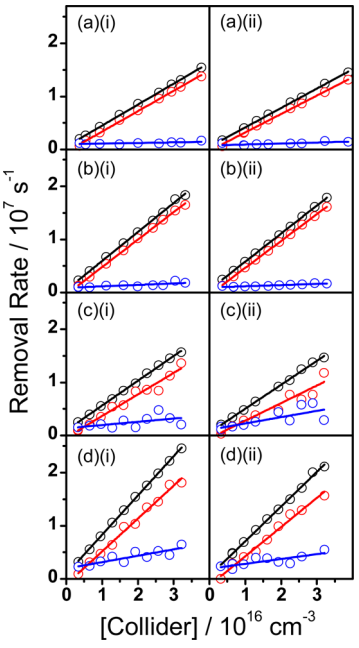

Figure 5. Population removal rates (open circles) as a function of collider number density, with linear fits. (Black) Total removal $\Gamma^{(0)}_{j,\mathrm{tot}}$; (red) reversible removal, $\Gamma^{(0)}_{j\rightarrow j'}$; (blue) irreversible removal, $\Gamma^{(0)}_{j\rightarrow x}$. (a) Ar; (b) N_2; (c) O_2; and (d) CO_2 colliders. Initial states (i) j = 6.5 F_1e and (ii) j = 11.5 F_1e.

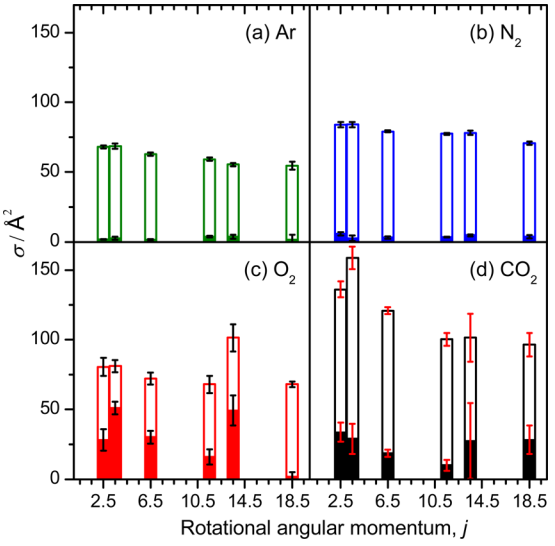

Figure 6. Stacked bar charts of the total removal cross sections, (a) Ar, (b) N_2, (c) O_2, and (d) CO_2. $\sigma^{(0)}_{j\rightarrow x}$ (filled bars), $\sigma^{(0)}_{j\rightarrow j'}$ (open bars), and σ_{pop} (summed bar). Error bars are 1σ standard errors from the independent fits. Results for Ar from measurements reported in ref 11.

Consistent with the observed differences in the long-time behavior of the kinetic traces for the different colliders and the second-order plots of the individual transfer rates shown in Figure 5, we find that for Ar and N_2, the total removal cross sections are completely dominated by transfer to states from which return is possible, $\sigma^{(0)}_{j\rightarrow j'}$. In contrast, for O_2 and CO_2, a substantial contribution to the total removal cross sections comes from $\sigma^{(0)}_{j\rightarrow x}$, representing removal to states from which return to the initial state does not occur. The $\sigma^{(0)}_{j\rightarrow j'}$ + $\sigma^{(0)}_{j\rightarrow x}$ (total bar height) shown in Figure 6a and b agree quantitatively with the σ_{pop} shown in Figure 4, but those in Figure 6c and d are in

dx.doi.org/10.1021/jp4123503 | J. Phys. Chem. A 2014, 118, 2007−2017

much poorer agreement with Figure 4. The uncertainties in the individual $\Gamma^{(0)}_{j\rightarrow j'}$ and $\Gamma^{(0)}_{j\rightarrow x}$ rates when both are of significant magnitude are found to be large and quite strongly correlated. This is visible in Figure 5c(i,ii) and d(i,ii) and leads to the substantial error bars shown in Figure 6c and d. In contrast, the total removal rates $\Gamma^{(0)}_{j,\mathrm{tot}}$ are well-determined, as shown by the second-order plots for $\Gamma^{(0)}_{j,\mathrm{tot}}$ in Figure 3 and Figure 5, leading to the small errors reported in Figure 4.

Finally, the state-to-state RET cross sections were determined. The state-to-state population transfer rate, $\Gamma^{(0)}_{j\rightarrow j'}$, determined by fitting individual product level kinetic traces to eq 7 as detailed above, was converted to a bimolecular state-to-state rate constant, $k^{(0)}_{j\rightarrow j'}$, by dividing by the collider number density (400 mTorr for O_2 and N_2 and 200 mTorr for CO_2), where it was assumed that the effect of the small pressure of ICN was negligible. This is a reasonable assumption given the near-zero intercept rates determined from the bimolecular plots shown in Figure 3. The independent multiple measurements of $k^{(0)}_{j\rightarrow j'}$ for each product level, typically 4−6 acquired on different days, were then averaged. The rate constants were again turned into thermally averaged cross sections and are compared for the different colliders in Figure 7, together with our previously published results for Ar.[10]

The state-to-state cross sections for both spin−orbit and Λ-doublet *Fε*-conserving and *Fε*-changing transitions in Figure 7 for all four colliders display a marked even/odd Δ*j* alternation, with even Δ*j* preferred for *Fε*-conserving transfer and odd-Δ*j* preferred for *Fε*-changing transitions. Similar overall transfer cross sections for the *Fε*-conserving transitions are observed for Ar and N_2, although there are detailed differences. Substantially smaller cross sections are observed for O_2 and CO_2 (note again the contrast with the trends in the total removal cross sections in Figure 4). In all cases, the cross sections for *Fε*-changing collisions are smaller than those for *Fε*-conserving, with all of the molecular colliders displaying *Fε*-changing cross sections that are approximately 1/2 of the magnitude of the respective *Fε*-conserving cross sections, in contrast to Ar, where the equivalent ratio is ∼1/3.

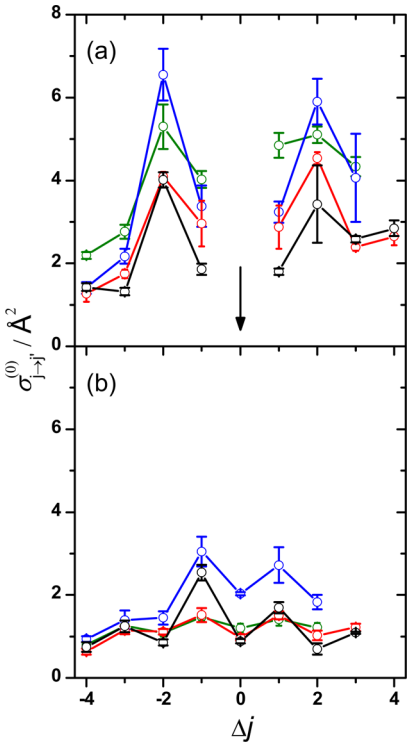

Figure 7. Thermally averaged state-to-state RET cross sections, $\sigma^{(0)}_{j\rightarrow j'}$, from initial level j = 6.5 F_1e (indicated by an arrow) for N_2 (blue), O_2 (red), and CO_2 (black) colliders for (a) spin−orbit- and Λ-doublet-conserving collisions and (b) spin−orbit- and Λ-doublet-changing collisions. Previous measurements for Ar (olive) from ref 10 are shown for comparison. The errors are the 1σ standard error of the mean from multiple independent measurements.

4. DISCUSSION

Total Removal Cross Sections. We first discuss the total removal cross sections as a function of collider, as shown in Figure 4. The only other rotationally resolved study of molecular colliders for which σ_{pop} has been reported is by Khachatrian and Dagdigian for collisions of CN(A) with N_2, although their measurements were for the adjacent ν = 3 vibrational level.[13] Figure 4 includes their experimental measurements for a range of j F_1f states, which are in quantitative agreement with our measurements. The order of the σ_{pop} for the different colliders is Ar < O_2 < N_2 < CO_2. This appears to be loosely correlated with long-range attractive dispersion and lowest-order electrostatic forces determined by polarizabilities and quadrupole moments, as listed in Table 1. It has commonly been argued that the larger absolute magnitude of the quadrupole moment of N_2 compared to O_2 is responsible for the larger cross sections in a variety of related phenomena, including the inelastic contribution to line broadening.[42,43]

Table 1. Dipole Moments (μ), Quadrupole Moments (Θ), and Polarizabilities (α) of CN($A^2\Pi$) and the Ar, N_2, O_2, and CO_2 Colliders

species	μ/D	Θ/D·Å	α/Å^3
CN($A^2\prod$)	0.3[a]	*b*	
Ar			1.66[e]
N_2		−1.40[c]	1.71[e]
O_2		−0.4[d]	1.56[e]
CO_2		−4.28[c]	2.51[e]

[a]Reference 44. [b]No literature value available. [c]Reference 45. [d]Reference 46. [e]Reference 47.

This straightforward long-range attractive-force argument might also be invoked to rationalize our results for CN(A) here. However, the basis of such an analysis has been questioned in systems such as OH(X) with N_2 and O_2, where rigorous calculations indicate a significantly deeper interaction with O_2.[48] Moreover, the breakdown of the removal cross sections into reversible and irreversible components shown in Figure 6 also cautions against an overly simplistic interpretation based on a common RET mechanism. There is strong evidence for a substantial fraction of the total rotationally resolved removal cross section with O_2 and CO_2 arising from either EET or reaction. Table 2 shows the literature vibrationally resolved total quenching rate constants, k_Q, for CN(A) with Ar, N_2, O_2, and CO_2, together with a Boltzmann-weighted average of the individual $k^{(0)}_{j\rightarrow x}$ rate constants derived from the breakdown shown in Figures 5 and 6. There is perhaps surprisingly good agreement between the literature k_Q and those determined by this method for Ar, N_2, and CO_2, given that our experimental design was not optimized for this measurement. There are no previous measurements of k_Q with O_2 for CN(A, ν = 4), and the rate constant that we observe is much faster (although with

dx.doi.org/10.1021/jp4123503 | J. Phys. Chem. A 2014, 118, 2007−2017

Table 2. Quenching Rate Constants, k_Q, for CN($A^2\Pi$, ν') in Collisions with Ar, N_2, O_2, and CO_2, from Literature Sources and from This Work (bold)

	$k_Q/10^{-11}$ cm^3 s^{-1}			
ν'	Ar	N_2	O_2	CO_2
0		0.044 ± 0.005[a]	3.0 ± 0.2[b]	
1		0.24 ± 0.015[b]	3.1 ± 0.1[b]	2.5 ± 0.15[b]
2	0.51 ± 0.1[c]	2.39 ± 0.2[c]		5.3 ± 0.5[c]
3	1.50 ± 0.2[c]	2.36 ± 0.2[c]		6.9 ± 0.7[c]
4	2.63 ± 0.2[c]	3.83 ± 0.3[c]		13.1 ± 1.0[c]
	1.6 ± 0.3	**2.6 ± 0.3**	**21 ± 5**	**14 ± 2**
5	3.03 ± 0.3[c]	4.43 ± 0.4[c]		7.8 ± 0.8[c]

[a]Reference 54. [b]Reference 28. [c]Reference 27.

large uncertainties) than that previously reported for CN(A, ν = 1).[28] The clear differences between the population decay traces at long delays observed for collisions with O_2 and N_2, combined with the good agreement between our k_Q and the literature value for N_2, give us confidence, however, that regardless of the large statistical uncertainties, total quenching of CN(A, ν = 4) with O_2 is a rapid process.

There is no direct information from this study on the partitioning of the total quenching between EET and reaction. The reaction of CN(X) with both O_2 and CO_2 is exothermic, and with an additional ∼190 kJ mol^{-1} of energy available for CN(A, ν = 4), reactive pathways must be energetically accessible for both colliders. CN(X) + O_2 is a prototypical barrierless radical−radical complex forming reaction, leading to NCO + O and NO + CO product channels, while CN(X) + CO_2 is much less studied and is believed to lead to NCO + CO products over a substantial barrier.[49,50] If the observed total quenching rate constant of 21 ± 5 × 10^{-11} cm^3 s^{-1} for CN(A) + O_2 does reflect reactive loss, then CN(A, ν = 4) is approximately an order of magnitude more reactive toward O_2 than CN(X) at room temperature, implying a strong electronic and vibrational state dependence.[28,49] While quenching with CO_2 could be reactive, a distinct argument has previously been presented to explain the CN(A) vibrational level dependence that suggests that it is primarily EET.[27] The energy gap between CN(A, ν = 4) and CN(X, ν = 7), ΔE = 2373 cm^{-1}, is near-resonant with the CO_2 ν_3 asymmetric stretching mode and may therefore facilitate rapid EET. Huang et al. showed that, except for ν = 4, EET from CN(A) only leads to the single vibrational level of CN(X) lying immediately below in energy, for example, CN(A, ν = 3) to CN(X, ν = 7), whereas for CN(A, ν = 4), EET was observed to both CN(X, ν = 8) and CN(X, ν = 7), supporting this proposal.[27] The cross sections for all colliders decline as a function of j, commonly observed and usually explained in terms of the increasing energy gaps between levels with increasing j and the limitations of linear to angular momentum transfer in inelastic collisions.[51] Closer inspection shows that the relative rate of decrease is considerably faster for CO_2 and O_2 than that for N_2 and Ar, with the ratios of $\sigma_{pop}(j = 2.5)/(j = 18.5)$ lying in the order N_2 (1:0.86) > Ar (1:0.83) > O_2 (1:0.77) > CO_2 (1:0.69). This may be evidence for a more strongly preferred orientation leading to total quenching for O_2 and CO_2, which is then washed out more effectively than that for the other colliders as the rotational speed of the CN increases.[52,53]

State-to-State Cross Sections. Comparison of the partner dependence of the state-to-state cross sections shown in Figure 7 with the total removal cross sections for the prepared j = 6.5 F_1e state in Figure 4 reinforces the discussion in the previous subsection regarding the behavior of the different colliders. Although we have not probed all of the product levels and therefore cannot directly compare the total population removal, σ_{pop}, to the sum of all RET processes, we have probed the majority of the significant open channels in the pure $F\varepsilon$-conserving and pure $F\varepsilon$-changing transitions. In the absence of any other information, we would expect the sum of the measured channels to represent approximately half of the total RET cross section, on the assumption that there will be a roughly equal combined population in the unobserved F-conserving/ε-changing and F-changing/ε-conserving channels. Here, we are assuming that conservation of rotational parity, rather than conservation of the Λ-doublet, is dominant in CN(A) collisions at low j, as previously observed in the CN(A)−Ar experiment and predicted by QS theory.[10,11,18] As Table 3 shows, we do indeed see excellent agreement with this assumption for Ar. We also see very good agreement for N_2, which is consistent with the small quenching cross sections obtained in this work and previously reported.[27] In contrast, for O_2 and, most dramatically, for CO_2, the sum of the state-to-state cross sections is less than half of σ_{pop}. This is consistent with another process removing the initial state, with a cross section of significant magnitude, which we presume to be quenching. However, the implied magnitudes of the cross sections for quenching by O_2 and CO_2 are, respectively, significantly smaller and much larger than those determined by the kinetic fitting and reported (as rate constants) in Table 2. There are substantial uncertainties in the sum of the state-to-state cross sections arising from unobserved levels within the measured $F\varepsilon$-conserving and $F\varepsilon$-changing channels, as well as the assumption regarding the unobserved F-conserving/ε-changing and F-changing/ε-conserving channels. The quenching rate constants reported in Table 2 should therefore be more reliable and represent our best estimates for this channel.

Table 3. Total Removal Cross Sections, σ_{pop}, from Figure 3 for j = 6.5 F_1e and the Sum of the Individual State-to-State Cross Sections, $\sum\sigma_{j-j'}$, for Transfer from j = 6.5 F_1e to All Measured j' F_1e and j' F_2f Product States[a]

collider	$\sum\sigma_{j-j'}$/Å^2	σ_{pop}/Å^2
Ar	36.99 ± 4.94	61.71 ± 1.61
N_2	40.11 ± 9.52	82.31 ± 0.64
O_2	31.66 ± 5.40	69.77 ± 1.37
CO_2	29.01 ± 5.28	121.56 ± 1.38

[a]Errors are 2σ.

We can compare the general form of our state-to-state cross sections for N_2 and CO_2 to those previously reported from experiments by Khachatrian et al.[13,14] They prepared different initial states, specifically ν = 3 j = 7.5 F_1f and ν = 3 j = 9.5 F_2f. We do not expect the difference in initial vibrational state to have a significant effect on the relative state-to-state rotational cross sections, although it may affect the overall absolute removal cross section.[10,11] Similarly, we do not believe that the small change in the initial state rotational energy and angular momentum, relative to the available collision energy and orbital angular momentum, will lead to substantial changes in relative state-to-state propensities when comparing the two studies. The N_2 and CO_2 relative state-to-state cross sections reported here show marked disagreements with the experimental results previously reported by Khachatrian et al.[13,14] For $F\varepsilon$-conserving

dx.doi.org/10.1021/jp4123503 | J. Phys. Chem. A 2014, 118, 2007−2017

relative cross sections, while the general decrease with increasing Δj is approximately the same as that observed by Khachatrian et al., they do not report the characteristic even−odd alternation corresponding to conservation of total parity that we observe and is predicted by theory for N_2. Further, we observe $F\epsilon$-changing cross sections that have the same general Δj dependence as those observed with Ar.[10] For both N_2 and CO_2, our $F\epsilon$-changing cross sections are approximately half of the magnitude of the $F\epsilon$-conserving cross sections, in contrast to the small or vanishing cross sections reported by Khachatrian et al.[13,14] Our cross sections for N_2 are in much better agreement with the QS calculations reported in ref 13. Given the high signal-to-noise of our measurements, the care that we have taken in ensuring reproducibility and to minimize the possibility of collider gas contamination, as well as the excellent agreement of our previous Ar measurements (taken using identical experimental protocols) with QS theory, we are confident that our reported $F\epsilon$-changing cross sections are robust. We therefore propose that the CN(A)−N_2 PESs and the QS calculations on them do, in fact, provide quite a good representation of the inelastic scattering, contrary to the conclusions of Khachatrian et al. We conclude that the disagreement between experiment and theory presented in ref 13 and the strong $F\epsilon$-conserving propensity reported for CO_2 in ref 14 must therefore more likely have arisen from some undetected experimental artifact. This apparent insensitivity of the inelastic scattering to the N_2 orientation is in contrast to the recently reported work of Kalugina et al. on the related CN(X)−H_2 system.[55] The full 4-d PES including the relative orientation of the H_2 collider was required to reproduce the experimentally measured state-to-state RET cross sections. Clearly, the ability of QS calculations on an averaged PES to reproduce experiment may not be universal and may depend on the nature of the system.

Relative spin−orbit-changing cross sections in Figure 7 are larger for all of the molecular colliders than those observed for Ar. This suggests that the V_{dif} PES is of larger magnitude in regions that are accessible at thermal collision energies for the molecular colliders. Perhaps surprisingly, no significant difference in the relative spin−orbit-changing cross sections is observed between N_2 and O_2. Clearly the open-shell electronic structure of the O_2 does not result in facile spin−orbit transfer for CN(A).

Strong even−odd Δj oscillations in the cross sections are seen in Figure 7 for all of the molecular colliders. This represents a preference for conservation of total parity, as has previously been observed in collisions of CN(A) with Ar.[10,18,56] As noted in the Introduction, within a weak coupling limit, the parity-conserving transfer arises from the even terms in the angular expansion of the PES, with the odd terms leading to parity-changing transfer. The strong propensity for parity conservation in CN(A) + Ar RET is thus a manifestation of the dominance of even terms in the angular expansion of the PES, itself a result of the near homonuclearity of CN.[18] The strong propensity for conservation of parity observed here in collisions with N_2, O_2, and CO_2 presumably reflects a similar dominance of even terms in the respective PESs, despite the additional dimensions introduced with these nonspherical colliders. The ab initio PESs presented by Khachatrian et al. for CN(A)−N_2 do indeed display a strong even order, and the associated QS calculations on spherically averaged CN(A)−N_2 PESs predicted a strong preference for parity conservation, consistent with our experimental measurements.[13] No ab initio PESs are available for CN(A)−O_2 and CN(A)−CO_2. The strong parity conservation preference also observed for these colliders implies that these PESs are also principally even in character. Notwithstanding the limitations of arguments based purely on long-range attractive forces expressed above, this would be consistent with the long-range PESs being dominated by quadrupole−quadrupole interactions.[14] As noted in Table 1, the dipole moment of CN(A) is relatively small, although there are no measurements or calculations of the CN(A) quadrupole moment, precluding any quantitative analysis of the balance between dipole−quadrupole and quadrupole−quadrupole interactions. However, similar parity conservation effects have been observed in low-temperature (7 K) collisions of CN(A) with H_2, suggesting that a strong even-order character to CN(A)−molecular collider PESs is not uncommon, at least with centrosymmetric colliders.[30] Significantly, in related experiments where CN(X)−H_2 complexes were excited to the A state and underwent predissociation to CN(A) + H_2, no such parity propensity was observed.[30,31] It was suggested that the restricted range of initial geometries available to the excited complex was responsible for the loss of parity conservation, demonstrating that parity conservation is indeed driven by specific symmetry elements of the PES.

As previously discussed, there is possible evidence in the j dependence of σ_{pop} for preferred quenching geometries for CN(A) + O_2/CO_2. A separate question is whether the parity-dependent state-to-state CN(A) + O_2/CO_2 measurements presented here provide additional evidence for such an anisotropy in the PESs. The answer appears to be no. The only significant differences in the scattering with O_2 and CO_2 compared to the inert N_2 lie in the j-dependent σ_{pop} and the overall breakdown between RET and quenching. There are no strong differences in the Δj dependence of the RET, and the magnitude of the parity-dependent oscillations are broadly similar for all colliders. There are very few full parity-resolved measurements for RET of $^2\Pi$ species with molecular colliders, particularly where potentially reactive and nonreactive colliders are compared. Hexapole state selection has been used in crossed molecular beam experiments to determine the state-to-state cross sections for RET of OH($X^2\Pi$, j = 3/2, F_1f) in collisions with CO, N_2, and CO_2.[8] A preference for parity conservation was observed with all three colliders for transfer into j' = 5/2 F_1 and 1/2 F_2, but no general parity propensity was otherwise observed. This may be the result of the much more heteronuclear nature of OH(X) and the consequent loss of even symmetry in the PESs. No significant differences were observed between N_2 and CO as colliders, despite the presence of the strongly attractive reactive pathway for OH(X)−CO, leading to H + CO_2. Similarly, comparison of experimental RET in OH(A) + Kr and QCT and QS calculations on an ab initio PES provided excellent agreement, despite the neglect of the electronic quenching channel in the calculations.[52] This suggests that more dynamically sensitive measurements are required to probe the geometry of reaction and quenching within the inelastically scattered products, such as the transfer of rotational angular momentum polarization[57,58] or measurements of differential scattering cross sections and product rotational angular momentum polarization.[59−61]

5. CONCLUSIONS

We have presented state-resolved removal cross sections and state-to-state RET cross sections for the collisions of CN(A, ν = 4) with N_2, O_2, and CO_2 at thermal collision energies. We

dx.doi.org/10.1021/jp4123503 | J. Phys. Chem. A 2014, 118, 2007−2017

observe a strong dependence on the collider for the total removal cross sections. There is clear evidence for an additional rapid removal channel for O_2 and CO_2, which may be electronic quenching or reaction. The magnitudes of the state-to-state RET cross sections support this interpretation. They display a strong preference for rotational parity conservation for all three colliders, similar to that previously observed with Ar.[10] These measurements are in stark contrast to the experimental measurements previously reported for N_2 and CO_2 but are in good agreement with QS calculations on ab initio PESs reported in the same work for N_2.[13,14] We therefore propose that some unrecognized experimental artifact must have been present in the previous work and that the calculations presented there were in fact in good agreement with experiment. If correct, a positive conclusion is that even approximate scattering calculations based on average potentials can, in fact, reproduce the essential features of the dynamics in this system. While this may prove to be an approximation too far in other cases, as with CN(X)−H_2,[55] we hope that its recognition might encourage the future expansion of the application of theory to such molecule−molecule collision studies.

AUTHOR INFORMATION

Corresponding Author

*E-mail: M.L.Costen@hw.ac.uk. Tel: +44 131 451 8197.

Present Address

‡J.B.H.: Department of Chemistry, Howard University, Washington, DC 20059, U.S.A.

Notes

The authors declare no competing financial interest.

ACKNOWLEDGMENTS

We thank David Georgiev for his contributions to the experimental measurements. S.J.M. thanks the Engineering and Physical Sciences Research Council for a Doctoral Training Award Ph.D. studentship. J.B.H. acknowledges the support of the National Science Foundation through Grant OISE-1157373.

REFERENCES

(1) Dagdigian, P. J. State-Resolved Collision-Induced Electronic Transitions. *Annu. Rev. Phys. Chem.* **1997**, *48*, 95−123.

(2) Schiffman, A.; Chandler, D. W. Experimental Measurements of State-Resolved, Rotationally Inelastic Energy-Transfer. *Int. Rev. Phys. Chem.* **1995**, *14*, 371−420.

(3) Gijsbertsen, A.; Linnartz, H.; Stolte, S. Parity-Dependent Rotational Rainbows in D_2−NO and He−NO Differential Collision Cross Sections. *J. Chem. Phys.* **2006**, *125*, 133112.

(4) Taatjes, C. A.; Gijsbertsen, A.; de Lange, M. J. L.; Stolte, S. Measurements and Quasi-Quantum Modeling of the Steric Asymmetry and Parity Propensities in State-to-State Rotationally Inelastic Scattering of NO ($^2\Pi_{1/2}$) with D_2. *J. Phys. Chem. A* **2007**, *111*, 7631−7639.

(5) Eyles, C. J.; Brouard, M.; Yang, C. H.; Klos, J.; Aoiz, F. J.; Gijsbertsen, A.; Wiskerke, A. E.; Stolte, S. Interference Structures in the Differential Cross-Sections for Inelastic Scattering of NO by Ar. *Nat. Chem.* **2011**, *3*, 597−602.

(6) Eyles, C. J.; Brouard, M.; Chadwick, H.; Hornung, B.; Nichols, B.; Yang, C. H.; Klos, J.; Aoiz, F. J.; Gijsbertsen, A.; Wiskerke, A. E.; et al. Fully Lambda-Doublet Resolved State-to-State Differential Cross-Sections for the Inelastic Scattering of NO(X) with Ar. *Phys. Chem. Chem. Phys.* **2012**, *14*, 5403−5419.

(7) Eyles, C. J.; Brouard, M.; Chadwick, H.; Aoiz, F. J.; Klos, J.; Gijsbertsen, A.; Zhang, X.; Stolte, S. The Effect of Parity Conservation on the Spin−Orbit Conserving and Spin−Orbit Changing Differential Cross Sections for the Inelastic Scattering of NO(X) by Ar. *Phys. Chem. Chem. Phys.* **2012**, *14*, 5420−5439.

(8) van Beek, M. C.; Schreel, K.; ter Meulen, J. J. Rotational Excitation of OH in Collisions with CO, N_2, and CO_2. *J. Chem. Phys.* **1998**, *109*, 1302−1309.

(9) Kirste, M.; Wang, X. A.; Schewe, H. C.; Meijer, G.; Liu, K. P.; van der Avoird, A.; Janssen, L. M. C.; Gubbels, K. B.; Groenenboom, G. C.; van de Meerakker, S. Y. T. Quantum-State Resolved Bimolecular Collisions of Velocity-Controlled OH with NO Radicals. *Science* **2012**, *338*, 1060−1063.

(10) McGurk, S. J.; McKendrick, K. G.; Costen, M. L.; Alexander, M. H.; Dagdigian, P. J. Parity-Dependent Oscillations in Collisional Polarization Transfer: CN($A^2\Pi$, ν = 4) + Ar. *J. Chem. Phys.* **2013**, *139*, 124304.

(11) McGurk, S. J.; McKendrick, K. G.; Costen, M. L.; Bennett, D. I. G.; Kłos, J.; Alexander, M. H.; Dagdigian, P. J. Depolarization of Rotational Angular Momentum in CN($A^2\Pi$, ν = 4) + Ar Collisions. *J. Chem. Phys.* **2012**, *136*, 164306.

(12) Ballingall, I.; Rutherford, M. F.; McKendrick, K. G.; Costen, M. L. Elastic Depolarization and Polarization Transfer in CN($A^2\Pi$, ν=4) + Ar Collisions. *Mol. Phys.* **2010**, *108*, 847−863.

(13) Khachatrian, A.; Dagdigian, P. J.; Bennett, D. I. G.; Lique, F.; Klos, J.; Alexander, M. H. Experimental and Theoretical Study of Rotationally Inelastic Collisions of CN($A^2\Pi$) with N_2. *J. Phys. Chem. A* **2009**, *113*, 3922−3931.

(14) Khachatrian, A.; Dagdigian, P. J. Rotationally Inelastic Collisions of CN($A^2\Pi$) with Small Molecules. *J. Phys. Chem. A* **2009**, *113*, 13390−13394.

(15) Alagappan, A.; Ballingall, I.; Costen, M. L.; McKendrick, K. G.; Paterson, G. Efficiencies of State and Velocity-Changing Collisions of Superthermal CN $A^2\Pi$ with He, Ar, N_2 and O_2. *Phys. Chem. Chem. Phys.* **2007**, *9*, 747−754.

(16) Alagappan, A.; Ballingall, I.; Costen, M. L.; McKendrick, K. G. Differential Scattering Cross-Sections for CN $A^2\Pi$+Ar. *J. Chem. Phys.* **2007**, *126*, 041103.

(17) Yang, X.; Dagdigian, P. J.; Alexander, M. H. Experimental and Theoretical Study of Rotationally Inelastic Collisions of Highly Rotationally Excited CN($A^2\Pi$) with Ar. *J. Chem. Phys.* **2000**, *112*, 4474−4484.

(18) Alexander, M. H.; Yang, X.; Dagdigian, P. J.; Berning, A.; Werner, H. J. Potential Energy Surfaces for the CN($X^2\Sigma^+$, $A^2\Pi$)−Ar System and Inelastic Scattering within the A State. *J. Chem. Phys.* **2000**, *112*, 781−791.

(19) Yang, X.; Dagdigian, P. J. Selective Rotational Energy Transfer from Individual Lambda-Doublet Levels of Highly Rotationally Excited CN($A^2\Pi$). *Chem. Phys. Lett.* **1998**, *297*, 506−514.

(20) Alexander, M. H. Quantum Treatment of Rotationally Inelastic-Collisions Involving Molecules in Π-Electronic States — New Derivation of the Coupling Potential. *Chem. Phys.* **1985**, *92*, 337−344.

(21) Brown, J. M.; Hougen, J. T.; Huber, K. P.; Johns, J. W. C.; Kopp, I.; Lefebvrebrion, H.; Merer, A. J.; Ramsay, D. A.; Rostas, J.; Zare, R. N. Labellign of Parity Doublet Levels in Linear Molecules. *J. Mol. Spectrosc.* **1975**, *55*, 500−503.

(22) Dagdigian, P. J.; Alexander, M. H.; Liu, K. The Inelastic-Scattering of $^2\Pi$-[Case(B)] Molecules and an Understanding of the Differing Lambda-Doublet Propensities for Molecules of Π vs $^3\Pi$ Orbital Occupancy. *J. Chem. Phys.* **1989**, *91*, 839−848.

(23) Alexander, M. H. Rotationally Inelastic-Collisions between a Diatomic Molecule in a $^2\Pi$ Electronic State and a Structureless Target. *J. Chem. Phys.* **1982**, *76*, 5974−5988.

(24) Orlikowski, T.; Alexander, M. H. Quantum Studies of Inelastic-Collisions of NO($X^2\Pi$) with Ar. *J. Chem. Phys.* **1983**, *79*, 6006−6016.

(25) Osborne, M. A.; McCaffery, A. J. A Fitting Law for Rotational Transfer Rates — An Angular-Momentum Model with Predictive Power. *J. Chem. Phys.* **1994**, *101*, 5604−5614.

(26) McCaffery, A. J.; Alwahabi, Z. T.; Osborne, M. A.; Williams, C. J. Rotational Transfer, An Angular-Momentum Model. *J. Chem. Phys.* **1993**, *98*, 4586−4602.
(27) Huang, Y. H.; Lu, R. C.; Halpern, J. B. Radiation and Collisional Energy-Transfer among the $A^2\Pi$ and $X^2\Sigma^+$ States of CN. *Appl. Opt.* **1993**, *32*, 981−986.
(28) Taherian, M. R.; Slanger, T. G. Quenching of CN($A^2\Pi$, ν=0,1) by O_2, H_2, N_2, NO, and CO_2. *J. Chem. Phys.* **1985**, *82*, 2511−2512.
(29) Halpern, J. B.; Huang, Y. Collisional Electronic Energy Transfer in CN Free Radicals. In *Research in Chemical Kinetics*; Compton, R. G., Hancock, G., Eds.; Elsevier: Amsterdam, The Netherlands, 1993; pp 347−387.
(30) Chen, Y. L.; Heaven, M. C. Comparison of Direct and Resonant Scattering for H_2+CN($A\ ^2\Pi$): Collisional Energy Transfer versus Predissociation of CN(A)−H_2 Complexes. *J. Chem. Phys.* **2000**, *112*, 7416−7424.
(31) Chen, Y. L.; Heaven, M. C. Spectroscopy and Dynamics of the H_2−CN van der Waals Complex. *J. Chem. Phys.* **1998**, *109*, 5171−5174.
(32) Alagappan, A.; Costen, M. L.; McKendrick, K. G. Frequency Modulated Spectroscopy as a Probe of Molecular Collision Dynamics. *Spectrochim. Acta, Part A* **2006**, *63*, 910−922.
(33) Marinakis, S.; Paterson, G.; Richmond, G.; Rockingham, M.; Costen, M. L.; McKendrick, K. G. Rotational Angular Momentum Polarization: The Influence of Stray Magnetic Fields. *J. Chem. Phys.* **2008**, *128*, 021101.
(34) Costen, M. L.; North, S. W.; Hall, G. E. Vector Signatures of Adiabatic and Diabatic Dynamics in the Photodissociation of ICN. *J. Chem. Phys.* **1999**, *111*, 6735−6749.
(35) Sims, I. R.; Queffelec, J. L.; Defrance, A.; Rebrionrowe, C.; Travers, D.; Bocherel, P.; Rowe, B. R.; Smith, I. W. M. Ultralow Temperature Kinetics of Neutral−Neutral Reactions — The Technique and Results for the Reactions CN+O_2 Down to 13 K and CN+NH_3 Down to 25 K. *J. Chem. Phys.* **1994**, *100*, 4229−4241.
(36) Nadler, I.; Mahgerefteh, D.; Reisler, H.; Wittig, C. The 266 nm Photolysis of ICN — Recoil Velocity Anisotropies and Nascent E,V,R,T Excitations for the CN + I($^2P_{3/2}$) and CN + I($^2P_{1/2}$) Channels. *J. Chem. Phys.* **1985**, *82*, 3885−3893.
(37) Fano, U.; Macek, J. H. Impact Excitation and Polarization of Emitted Light. *Rev. Mod. Phys.* **1973**, *45*, 553−573.
(38) Blum, K. *Density Matrix Theory and Applications*, 2nd ed.; Plenum Press: New York, 1996.
(39) Costen, M. L.; Hall, G. E. Coherent and Incoherent Orientation and Alignment of ICN Photoproducts. *Phys. Chem. Chem. Phys.* **2007**, *9*, 272−287.
(40) Uberna, R.; Hinchliffe, R. D.; Cline, J. I. Photofragment μ−ν−J Correlation Measured by 1+N′ Resonance-Enhanced Multiphoton Ionization — Selective Probing of Bipolar Moments and Setection of Chiral Dynamics. *J. Chem. Phys.* **1995**, *103*, 7934−7945.
(41) North, S. W.; Zheng, X. S.; Fei, R.; Hall, G. E. Line Shape Analysis of Doppler Broadened Frequency-Modulated Line Spectra. *J. Chem. Phys.* **1996**, *104*, 2129−2135.
(42) Schiffman, A.; Nesbitt, D. J. Pressure Broadening and Collisional Narrowing in OH(ν=1−0) Rovibrational Transitions with Ar, He, O_2, and N_2. *J. Chem. Phys.* **1994**, *100*, 2677−2689.
(43) Benec'h, S.; Buldyreva, J.; Chrysos, A. Pressure Broadening and Temperature Dependence of Microwave and Far Infrared Rotational Lines in OH Perturbed by N_2, O_2, and Ar. *J. Mol. Spectrosc.* **2001**, *210*, 8−17.
(44) Knowles, P. J.; Werner, H. J.; Hay, P. J.; Cartwright, D. C. The $A^2\Pi$−$X^2\Sigma^+$ Red and $B^2\Sigma^+$−$X^2\Sigma^+$ Violet Systems of the CN Radical — Accurate Multireference Configuration-Interaction Calculations of the Radiative Transition-Probabilities. *J. Chem. Phys.* **1988**, *89*, 7334−7343.
(45) Graham, C.; Imrie, D. A.; Raab, R. E. Measurement of the Electric Quadrupole Moments of CO_2, CO, N_2, Cl_2 and BF_3. *Mol. Phys.* **1998**, *93*, 49−56.
(46) Buckingham, A. D.; Disch, R. L.; Dunmur, D. A. Quadrupole Moments of Some Simple Molecules. *J. Am. Chem. Soc.* **1968**, *90*, 3104.
(47) Olney, T. N.; Cann, N. M.; Cooper, G.; Brion, C. E. Absolute Scale Determination for Photoabsorption Spectra and the Calculation of Molecular Properties using Dipole Sum Rules. *Chem. Phys.* **1997**, *223*, 59−98.
(48) Paterson, G.; Marinakis, S.; Costen, M. L.; McKendrick, K. G. Depolarisation of Rotational Orientation and Alignment of OH ($X^2\Pi$) in Collisions with Molecular Partners: N_2 and O_2. *Phys. Chem. Chem. Phys.* **2009**, *11*, 8813−8820.
(49) Feng, W. H.; Hershberger, J. F. Reinvestigation of the Branching Ratio of the CN + O_2 Reaction. *J. Phys. Chem. A* **2009**, *113*, 3523−3527.
(50) Balla, R. J.; Casleton, K. H. Kinetic-Study of the Reactions of CN with O_2 and CO_2 from 292 to 1500 K Using High-Temperature Photochemistry. *J. Phys. Chem.* **1991**, *95*, 2344−2351.
(51) McCaffery, A. J.; Proctor, M. J.; Whitaker, B. J. Rotational Energy-Transfer — Polarization and Scaling. *Annu. Rev. Phys. Chem.* **1986**, *37*, 223−244.
(52) Chadwick, H.; Brouard, M.; Chang, Y. P.; Eyles, C. J.; Perkins, T.; Seamons, S. A.; Klos, J.; Alexander, M. H.; Aoiz, F. J. A New Potential Energy Surface for OH($A\ ^2\Sigma^+$)−Kr: The van der Waals Complex and Inelastic Scattering. *J. Chem. Phys.* **2012**, *137*, 154305.
(53) Lehman, J. H.; Lester, M. I.; Kłos, J.; Alexander, M. H.; Dagdigian, P. J.; Herráez-Aguilar, D.; Aoiz, F. J.; Brouard, M.; Chadwick, H.; Perkins, T.; Seamons, S. A. Electronic Quenching of OH $A\ ^2\Sigma^+$ Induced by Collisions with Kr Atoms. *J. Phys. Chem. A* **2013**, *117*, 13481−13490.
(54) Conley, C.; Halpern, J. B.; Wood, J.; Vaughn, C.; Jackson, W. M. Laser Excitation of the CN $B^2\Sigma^+$−$A^2\Pi$ 0−0 and 1−0 Bands. *Chem. Phys. Lett.* **1980**, *73*, 224−227.
(55) Kalugina, Y.; Klos, J.; Lique, F. Collisional Excitation of CN($X\ ^2\Sigma^+$) by para- and ortho-H_2: Fine-Structure Resolved Transitions. *J. Chem. Phys.* **2013**, *139*, 074301.
(56) Jihua, G.; Ali, A.; Dagdigian, P. J. State-to-State Collisional Interelectronic and Intraelectronic Energy Transfer Involving CN $A^2\Pi$ ν=3 and $X^2\Sigma^+$ ν=7 Rotational Levels. *J. Chem. Phys.* **1986**, *85*, 7098−7105.
(57) Paterson, G.; Costen, M. L.; McKendrick, K. G. Collisional Depolarisation of Rotational Angular Momentum: Influence of the Potential Energy Surface on the Collision Dynamics? *Int. Rev. Phys. Chem.* **2012**, *31*, 69−109.
(58) Brouard, M.; Chadwick, H.; Chang, Y. P.; Eyles, C. J.; Aoiz, F. J.; Klos, J. Collisional Angular Momentum Depolarization of OH(A) and NO(A) by Ar: A Comparison of Mechanisms. *J. Chem. Phys.* **2011**, *135*, 084306.
(59) Steill, J. D.; Kay, J. J.; Paterson, G.; Sharples, T. R.; Klos, J.; Costen, M. L.; Strecker, K. E.; McKendrick, K. G.; Alexander, M. H.; Chandler, D. W. Rotational Alignment of NO ($A^2\Sigma^+$) from Collisions with Ne. *J. Phys. Chem. A* **2013**, *117*, 8163−8174.
(60) Kay, J. J.; Steill, J. D.; Klos, J.; Paterson, G.; Costen, M. L.; Strecker, K. E.; McKendrick, K. G.; Alexander, M. H.; Chandler, D. W. Collisions of Electronically Excited Molecules: Differential Cross-Sections for Rotationally Inelastic Scattering of NO($A^2\Sigma^+$) with Ar and He. *Mol. Phys.* **2012**, *110*, 1693−1703.
(61) Kay, J. J.; Paterson, G.; Costen, M. L.; Strecker, K. E.; McKendrick, K. G.; Chandler, D. W. Communication: Direct Angle-Resolved Measurements of Collision Dynamics with Electronically Excited Molecules: NO($^2\Sigma^+$)+Ar. *J. Chem. Phys.* **2011**, *134*, 091101.